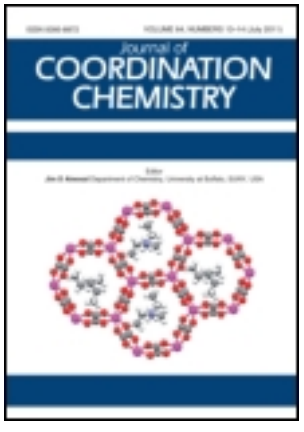

Journal of Coordination Chemistry
Publication details, including instructions for authors and subscription information:
http://www.tandfonline.com/loi/gcoo20

Self-assembled biomimetic catalysts: studies of the catalase and peroxidase activities of Mn(III)-Schiff base complexes

M. Ángeles Vázquez-Fernández [a], M. Isabel Fernández-García [a], Gustavo González-Riopedre [a], Marcelino Maneiro [a] & M. Jesús Rodríguez-Doutón [b]

[a] Departamento de Química Inorgánica, Facultade de Ciencias, Universidade de Santiago de Compostela, Avda. Alfonso X, Lugo E-27002, Spain

[b] Department of Chemistry and INSTM Research Unit, University of Modena and Reggio Emilia, Via G. Campi 183, 41100 Modena, Italy

Published online: 04 Nov 2011.

To cite this article: M. Ángeles Vázquez-Fernández, M. Isabel Fernández-García, Gustavo González-Riopedre, Marcelino Maneiro & M. Jesús Rodríguez-Doutón (2011) Self-assembled biomimetic catalysts: studies of the catalase and peroxidase activities of Mn(III)-Schiff base complexes, Journal of Coordination Chemistry, 64:22, 3843-3858, DOI: 10.1080/00958972.2011.633164

To link to this article: http://dx.doi.org/10.1080/00958972.2011.633164

Journal of Coordination Chemistry
Vol. 64, No. 22, 20 November 2011, 3843–3858

Self-assembled biomimetic catalysts: studies of the catalase and peroxidase activities of Mn(III)-Schiff base complexes

M. ÁNGELES VÁZQUEZ-FERNÁNDEZ†,
M. ISABEL FERNÁNDEZ-GARCÍA*†, GUSTAVO GONZÁLEZ-RIOPEDRE†,
MARCELINO MANEIRO*† and M. JESÚS RODRÍGUEZ-DOUTÓN‡

†Departamento de Química Inorgánica, Facultade de Ciencias, Universidade de Santiago de Compostela, Avda. Alfonso X, Lugo E-27002, Spain
‡Department of Chemistry and INSTM Research Unit, University of Modena and Reggio Emilia, Via G. Campi 183, 41100 Modena, Italy

(*Received 29 July 2011; in final form 29 September 2011*)

Five Mn(III) nitrate complexes have been synthesized from dianionic hexadentate Schiff bases obtained by the condensation of 3-ethoxy-2-hydroxybenzaldehyde with different diamines. The complexes have been characterized by elemental analysis, ESI mass spectrometry, IR and ^{1}H NMR spectroscopy, r. t. magnetic, and molar conductivity measurements. Parallel-mode EPR spectroscopy of **1** is also reported. Ligand H_2L^3 and complexes $[MnL^1(H_2O)_2](NO_3)(CH_3OH)$ (**1**), $[MnL^3(H_2O)_2]_2(NO_3)_2(CH_3OH)(H_2O)$ (**3**), and $[MnL^4(H_2O)_2](NO_3)(H_2O)_2$ (**4**) were crystallographically characterized. The X-ray structures show the self-assembly of the Mn(III)–Schiff base complexes through μ-aquo bridges between neighboring axial water molecules and also by π–π stacking interactions, establishing dimeric and polymeric structures. The peroxidase and catalase activities of the complexes have been studied. Complexes with the shorter spacer between the imine groups (**1**–**2**) behave as better peroxidase and catalase mimics, probably due to their ability to coordinate the hydrogen peroxide substrate to manganese.

Keywords: Manganese; Schiff bases; Supramolecular structure; Catalase; Peroxidase

1. Introduction

Manganese complexes involving tetradentate ONNO Schiff bases are one of the most versatile and interesting synthetic systems that can act as artificial mimics of peroxidases and catalases [1, 2]. Catalases are able to disproportionate H_2O_2 into water and dioxygen [3]; peroxidases catalyse oxidation of a broad range of substrates by hydrogen peroxide [4]. These enzymes protect organisms against oxidative stress by removing the appreciable levels of hydrogen peroxide, a by-product of respiration [5].

In our continuing research using Mn(III)–Schiff base as biomimetic models of several enzymes [6–9], we report here five complexes stabilized with nitrate counterions. Our scheme consists of obtaining ionic compounds in order to enhance their solubility

*Corresponding authors. Email: misabel.fernandez.garcia@usc.es; marcelino.maneiro@usc.es

ISSN 0095-8972 print/ISSN 1029-0389 online © 2011 Taylor & Francis
http://dx.doi.org/10.1080/00958972.2011.633164

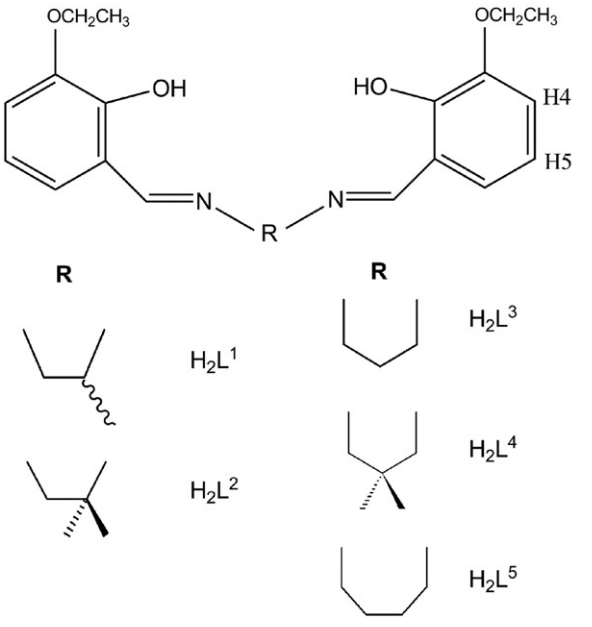

Scheme 1. Structures of the Schiff base ligands.

in alcoholic or aqueous solutions; hence their catalytic activity in this media should also be usable.

There are few examples of Mn(III)–Schiff base (or porphyrin) complexes with the nitrate anion. Of those found in the literature, some incorporate the ion to the first coordination sphere [10]; the nitrate group may also bridge manganese ions in Mn–carboxylate complexes [11], but there are a small number of cases where the nitrate acts as counterion in these type of systems [12, 13]. We have also previously added nitrate groups to Mn(III)–Gd(III)–Schiff base complexes, but this anion stabilized joining the Gd [14].

On the other hand, the ability of these anions for establishing hydrogen bonds would lead to new supramolecular architectures [15, 16]. The key role of anions in tuning the resultant structural topologies is a growing area of interest [17], and also its potential effect on the catalytic activity of this type of compounds is less studied. The selected Schiff-base ligands, H_2L^n (Scheme 1), contain six potential donors. They have an inner compartment with two imine nitrogens and two phenol oxygens in common and present two outer ethoxy groups, which may be involved in supramolecular interactions.

2. Experimental

2.1. *Materials*

All starting materials (Aldrich) and solvents (Probus) used for syntheses were commercially available reagent grade and used without purification.

2.2. *Physical measurements*

Elemental analyses were performed on a Carlo Erba Model 1108 CHNS-O elemental analyzer. IR spectra were recorded as KBr pellets on a Bio-Rad FTS 135 spectrophotometer from 4000 to 400 cm^{-1}. ^1H and ^{13}C NMR spectra were recorded on a Bruker AC-300 spectrometer using DMSO-d_6 (296 K) as solvent and $SiMe_4$ as an internal reference. The electro-spray mass spectra of the compounds were obtained on a Hewlett-Packard model LC-MSD 1100 instrument (positive ion mode, 98:2 CH_3OH–HCOOH as mobile phase, 30–100 V). Room-temperature magnetic susceptibilities were measured using a digital measurement system MSB-MKI, calibrated using mercury tetrakis(isothiocyanato)cobaltate(II) $Hg[Co(NCS)_4]$ as a susceptibility standard. Electronic spectra were recorded on a Cary 230 spectrometer. Conductivities of 10^{-3} mmol solutions in DMF were measured on a Crison microCM 2200 conductivity meter. EPR measurements were carried out on a Bruker ESP300E X-band spectrometer equipped with an ER4116 DM dual-mode cavity and an Oxford 900 continuous flow cryostat.

2.3. *Preparation of the Schiff bases*

All the Schiff bases used in this study were prepared by the condensation of the appropriate diamine with 3-ethoxy-2-hydroxybenzaldehyde. H_2L^1–H_2L^4 have been already reported and characterized by standard techniques [6, 8, 18]. The crystal structure of H_2L^3 is described in this work after obtaining crystals adequate for X-ray diffraction studies by slow evaporation of their respective methanol solutions. H_2L^5 was prepared by the method outlined below. It was characterized by elemental analysis, ^1H and ^{13}C NMR spectroscopy, ESI mass spectrometry, and IR spectroscopy.

H_2L^5: 1.00 g (6.02 mmol) of 3-ethoxy-2-hydroxybenzaldehyde and 0.30 mL (3.01 mmol) of 1,4-diaminobutane. m.p. 135°C. Anal. Calcd for $C_{22}H_{28}N_2O_4$ (384.5) (%): C, 68.7; H, 7.3; N, 7.3. Found (%): C, 69.0; H, 7.5; N, 7.3. MS ESI (*m*/*z*): 385. IR (KBr, cm^{-1}): ν(O–H) 3092 (m), ν(C=N) 1624 (vs), ν(C–O) 1248 (s). ^1H NMR (DMSO-d_6, ppm): δ 1.31 (t, 6H), 1.71 (q, 4H), 3.64 (t, 4H), 4.01 (c, 4H), 6.75 (t, 2H), 6.99 (d, 2H), 7.01 (d, 2H), 8.54 (s, 2H), 13.99 (br). ^{13}C NMR (DMSO-d_6, ppm): δ 15.0 (–CH_3), 28.2 (–CH_2–), 57.4 (=N–CH_2–), 64.2 (–OCH_2–), 116.3–123.5 (*C*ar), 147.5 (*C*–OH), 152.7 (*C*–OCH_2CH_3), 166.2 (*C*=N).

2.4. *Complex preparation*

All the Mg(III)–Schiff base complexes were prepared by stirring a methanol solution (50 mL) of the corresponding ligand and adding subsequently a methanol solution (30 mL) of $Mn(NO_3)_2 \cdot 4H_2O$ at room temperature. The initial light color of the solutions rapidly changed to brown. After 3 h of stirring at room temperature, slow evaporation of solvent leads to deposition of brown compounds. The products were collected by filtration, washed with diethyl ether (2×20 mL) and then dried *in vacuo*. Yields of the complexes vary, but are typically on the order of 70%.

$[MnL^1(H_2O)_2](NO_3)(CH_3OH)$ (1): H_2L^1 (0.20 g, 0.54 mmol); $Mn(NO_3)_2 \cdot 4H_2O$ (0.14 g, 0.54 mmol); yield: 0.19 g (65%). Anal. Calcd for $C_{22}H_{32}MnN_3O_{10}$ (553.45) (%): C, 47.7;

H, 5.7; N, 7.6. Found (%): C, 47.0; H, 5.7; N, 7.7. MS ESI (*m*/*z*): 423 $[MnL^1]^+$, 908 $[Mn_2L^1_2(NO_3)]^+$. IR (KBr, cm^{-1}): ν(O–H) 3425 (m), ν(C=N) 1616 (vs), ν(C–O) 1253 (s), $\nu(NO_3)$ 1384 (vs), 852 (m), 740 (s). ^{1}H NMR (DMSO-d_6, ppm): δ −30.09 (H4), −17.50, −20.63 (H5). $\Lambda_M = 68\,\mu S$.

$[MnL^2(H_2O)_2](NO_3)(H_2O)$ (2): H_2L^2 (0.20 g, 0.52 mmol); $Mn(NO_3)_2 \cdot 4H_2O$ (0.14 g, 0.52 mmol); yield: 0.20 g (70%). Anal. Calcd for $C_{22}H_{32}MnN_3O_{10}$ (553.4) (%): C, 47.7; H, 5.8; N, 7.6. Found (%): C, 47.2; H, 5.6; N, 7.6. MS ESI (*m*/*z*): 437 $[MnL^2]^+$, 936 $[Mn_2L^2_2(NO_3)]^+$. IR (KBr, cm^{-1}): ν(O–H) 3427 (m), ν(C=N) 1610 (vs), ν(C–O) 1254 (s), $\nu(NO_3)$ 1384 (vs), 855 (m), 738 (s). ^{1}H NMR (DMSO-d_6, ppm): δ −27.30 (H4), −17.40, −18.48 (H5). $\Lambda_M = 71\,\mu S$.

$[MnL^3(H_2O)_2]_2(NO_3)_2(CH_3OH)(H_2O)$ (3): H_2L^3 (0.25 g, 0.68 mmol); $Mn(NO_3)_2 \cdot 4H_2O$ (0.18 g, 0.68 mmol); yield: 0.29 g (79%). Anal. Calcd for $C_{43}H_{62}Mn_2N_6O_{20}$ (1092.84) (%): C, 47.2; H, 5.7; N, 7.7. Found (%): C, 46.3; H, 5.7; N, 7.5. MS ESI (*m*/*z*): 423 $[MnL^3]^+$, 908 $[Mn_2L^3_2(NO_3)]^+$. IR (KBr, cm−^{1}): ν(O–H) 3427 (m), ν(C=N) 1609 (vs), ν(C–O) 1254 (s), $\nu(NO_3)$ 1384 (vs), 850 (m), 739 (s). ^{1}H NMR (DMSO-d_6, ppm): δ −21.97 (H4), −18.00 (H5). $\Lambda_M = 68\,\mu S$.

$[MnL^4(H_2O)_2](NO_3)(H_2O)_2$ (4): H_2L^4 (0.20 g, 0.50 mmol); $Mn(NO_3)_2 \cdot 4H_2O$ (0.13 g, 0.50 mmol); yield: 0.25 g (85%). Anal. Calcd for $C_{23}H_{36}MnN_3O_{11}$ (585.5) (%): C, 47.2; H, 6.2; N, 7.2. Found (%): C, 46.9; H, 6.1; N, 7.2. MS ESI (*m*/*z*): 451 $[MnL^4]^+$, 964 $[Mn_2L^4_2(NO_3)]^+$. IR (KBr, cm^{-1}): ν(O–H) 3395 (m), ν(C=N) 1612 (vs), ν(C–O) 1258 (s), $\nu(NO_3)$ 1384 (vs), 840 (m), 739 (s). ^{1}H NMR (DMSO-d_6, ppm): δ −20.73 (H4), −16.75 (H5). $\Lambda_M = 86\,\mu S$.

$[MnL^5(H_2O)_2](NO_3)(H_2O)$ (5): H_2L^5 (0.25 g, 0.65 mmol); $Mn(NO_3)_2 \cdot 4H_2O$ (0.17 g, 0.52 mmol); yield: 0.24 g (83%). Anal. Calcd for $C_{22}H_{32}MnN_3O_{10}$ (553.4) (%): C, 47.7; H, 5.8; N, 7.6. Found (%): C, 47.8; H, 5.6; N, 7.6. MS ESI (*m*/*z*): 437 $[MnL^5]^+$, 936 $[Mn_2L^5_2(NO_3)]^+$. IR (KBr, cm^{-1}): ν(O–H) 3410 (m), ν(C=N) 1613 (vs), ν(C–O) 1254 (s), $\nu(NO_3)$ 1384 (vs), 858 (m), 740 (s). ^{1}H NMR (DMSO-d_6, ppm): δ −29.80 (H4), −21.05 (H5). $\mu = 5.0$ BM. $\Lambda_M = 67\,\mu S$.

2.5. *Peroxidase probes*

Oxidation of 2,2′-azinobis-(3-ethylbenzothiazoline)-6-sulfonic acid (ABTS) with H_2O_2 at *ca* pH 7 in the presence of the complexes was tested in the following manner. An aqueous solution of ABTS (50 µL; 0.009 M; 4.5×10^{-7} mol) and a methanolic solution of the complex (10 µL; 10^{-3} mmol; 10^{-8} mol) were added to water (3 mL). The intensity of the UV absorption bands of ABTS started to increase immediately after the addition of an aqueous solution of H_2O_2 (50 µL; 10 mmol; 5×10^{-4} mol).

2.6. *Studies on catalase-like function*

A 10 mL flask containing the solution of the complexes in methanol (3 mL, 1 mM) was sealed with a septum and connected to a gas-measuring burette (precision of 0.1 mL) through a double-ended needle. The solution was stirred at constant temperature on a water bath. The catalysis was initiated by introducing H_2O_2 solution (1 mL, 2.5 M) using a syringe, and the evolved dioxygen was volumetrically measured.

2.7. *Crystallographic data collection and refinement of the structure*

Single crystals of H_2L^3 and **1**, **3**, and **4**, suitable for X-ray diffraction studies, were obtained by slow evaporation of the methanolic solution at room temperature.

Detailed crystal data collection and refinement are summarized in table 1. Intensity data were collected on an Enraf-Nonius FR590 diffractometer using graphite-monochromated Cu-Kα radiation ($\lambda = 1.54184$ Å) for H_2L^3 at room temperature; on a Bruker-Smart CCD-1000 diffractometer employing graphite-monochromated Mo-Kα radiation ($\lambda = 0.71073$ Å) for **1** and **3** at room temperature, and for **4** at 110 K. The structures were solved by direct methods [19] and finally refined by full-matrix least-squares based on F^2. An empirical absorption correction was applied using SADABS [20]. All hydrogen atoms were included in the model at geometrically calculated positions.

3. Results and discussion

3.1. *Synthesis and characterization of the complexes*

Manganese(III) complexes (**1**–**5**) were prepared as detailed in section 2. They appear to be stable in the solid state and in solution, and they are moderately soluble in common organic solvents and soluble in polar aprotic coordinating solvents such as DMF and DMSO. Elemental analysis establishes their general formulas as $[MnL(H_2O)_2](NO_3)(D)_n$ ($D = H_2O$ or CH_3OH). These formulations are in agreement with molar conductivity measurements in 10^{-3} mmol DMF solutions, which are in the range of 67–86 $\mu S\,cm^{-1}$, indicating behavior attributable to 1 : 1 electrolytes [21]. Furthermore, other spectroscopic techniques support such formula and give insights into both solid and solution structure of the complexes.

All the complexes show similar IR spectra, exhibiting a strong band between 1616 and 1609 cm^{-1} characteristic of the ν(C=N) stretching mode, which is shifted 8–17 cm^{-1} lower with respect to the free Schiff base, indicating coordination to manganese through nitrogen of the imine group. The band attributed to ν(C–O) shifts 4–8 cm^{-1} to higher frequencies with respect to the free ligand. These data suggest the coordination of the Schiff bases through the inner phenol oxygens and the imine nitrogens. Strong bands centered at *ca* 3400 cm^{-1} can be assigned to a combination of ν(O–H) of coordinated and lattice water/methanol, now present in the complexes. The appearance of a new strong and sharp band at 1384 cm^{-1}, together with bands at *ca* 740 and 850 cm^{-1}, is characteristic of the presence of the non-coordinated nitrate [22].

ESI mass spectra registered in methanol show peaks corresponding to the fragment $[MnL]^+$ for all the complexes, indicating coordination of the Schiff base ligand to the metal centre. Other minor signals could be assigned to $[Mn_2L_2(NO_3)]^+$ units, which could be attributed to the presence of dimeric species.

The $\chi_M T$ values of all five complexes at room temperature are nearly equal and lie in the range of 5.91–6.16 $cm^3\,mol^{-1}\,K$. These results are in agreement with the expected contribution of two non-interacting or weakly interacting high-spin Mn^{III} ions (theoretical spin-only $\chi_M T$ value per dinuclear Mn^{III} unit = 6.00 $cm^3\,mol^{-1}\,K$ for $g = 2.00$). Such behavior is typical for this class of compounds. Previous magnetic studies on related compounds between 300 and 5 K indicated little or no

Table 1. Crystal data and structure refinement for H_2L^3, **1**, **3**, and **4**.

	1	**3**	**4**	H_2L^3
Empirical formula	$C_{22}H_{32}MnN_3O_{10}$	$C_{43}H_{62}Mn_2N_6O_{20}$	$C_{23}H_{36}MnN_3O_{11}$	$C_{21}H_{26}N_2O_4$
Formula weight	553.45	1092.84	585.49	370.44
Temperature (K)	293(2)	293(2)	110(2)	293(2)
Wavelength (Å)	0.71073	0.71073	0.71073	0.71073
Crystal system	Triclinic	Triclinic	Triclinic	Monoclinic
Space group	$P\bar{1}$	$P\bar{1}$	$P\bar{1}$	$P2_1/c$
Unit cell dimensions (Å, °)				
a	9.9779(25)	12.80(3)	7.8808(18)	10.024(5)
b	11.8256(30)	13.45(3)	13.052(3)	17.794(5)
c	12.8719(32)	15.38(3)	14.502(3)	11.761(5)
α	116.872(4)	91.41(4)	113.046(4)	90
β	105.001(4)	95.75(4)	92.638(4)	101.485(5)
γ	93.161(4)	107.15(3)	103.791(4)	90
Volume [Å^3]	1282.3 (6)	2513(9)	1316.8(5)	2055.8(15)
Z	2	2	2	4
Calculated density (Mg m^{-3})	1.433	1.442	1.477	1.197
Absorption coefficient (mm^{-1})	0.573	0.584	0.565	0.083
$F(000)$	580	1140	616	792
θ range for data collection (°)	1.87–27.22	1.33–23.26	1.54–26.37	2.07–24.71
Reflections collected	15,155	21,750	15,141	3614
Independent reflection	5655 [R(int) = 0.034]	7213 [R(int) = 0.0295]	5357 [R(int) = 0.0345]	3437 [R(int) = 0.0173]
Restraints/parameters	6/370	0/701	0/379	0/249
Goodness-of-fit on F^2	1.069	1.033	1.038	1.018
Final R indices [$I > 2\sigma(I)$]	$R_1 = 0.0515$, $wR_2 = 0.1425$	$R_1 = 0.0439$, $wR_2 = 0.1126$	$R_1 = 0.0331$, $wR_2 = 0.0724$	$R_1 = 0.0515$, $wR_2 = 0.1397$
R indices (all data)	$R_1 = 0.076$, $wR_2 = 0.1537$	$R_1 = 0.0651$, $wR_2 = 0.1276$	$R_1 = 0.0499$, $wR_2 = 0.0796$	$R_1 = 0.1231$, $wR_2 = 0.1720$

antiferromagnetic interaction between the metal centres [18, 23]. The room temperature magnetic moments observed in this study do not give cause to suppose that any different magnetic behavior should occur.

The electronic spectroscopic data recorded are very similar for **1**–**5**. A broad shoulder at 520–600 nm ($\varepsilon = 120$–$500\,(\text{mmol})^{-1}\,\text{cm}^{-1}$) is attributable to a d–d transition, while it is reasonable to assign the broad band at 480–490 nm ($\varepsilon = 2600$–$3300\ (\text{mmol})^{-1}\,\text{cm}^{-1}$) to the phenolate $\rightarrow$ Mn(III) charge-transfer. The peak at 300 nm ($\varepsilon = 21{,}000$–$23{,}000\,(\text{mmol})^{-1}\,\text{cm}^{-1}$) can be assigned to intraligand π–π^*. The energy and intensity of the LMCT and d–d transitions are in agreement with those reported for related Mn^{III} complexes [24, 25].

3.2. *^{1}H NMR studies of the complexes*

Spectra of the paramagnetic ^{1}H NMR of the complexes contain between two and three upfield proton resonances outside the diamagnetic region ($\delta = 0$–14 ppm) and are due to the isotropically shifting ligand protons for high-spin manganese(III) complexes in an octahedral field [26]. The signals must arise from the H4 and H5 protons of the aromatic phenoxy rings. The signals between -20.73 and -30.52 ppm are due to the H4 protons, while the resonances from -15.70 to -21.50 ppm are due to H5 protons. The signal corresponding to the H5 protons in **1** and **2** appears to be split into a doublet owing to the asymmetric nature of H_2L^1 and H_2L^2 Schiff bases. The ^{1}H NMR data serve to substantiate the formation of the manganese(III) complexes.

3.3. *EPR spectroscopy*

Parallel-mode EPR allows further insight into the structure of **1**. This technique enables one-electron $\Delta M_S = 0$ transitions to be detected that are hardly observable with a conventional EPR method ($H_1 > H_0$, perpendicular mode). Mn^{3+} has an integer electron spin, $S = 2$, and has been shown for powdered samples to develop a characteristic sextet pattern in parallel-mode EPR [27]. Figure 1 shows the spectrum

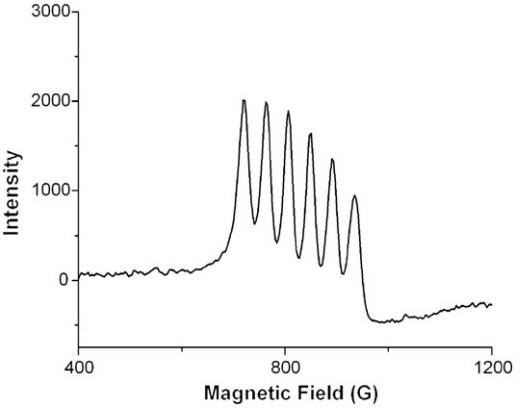

Figure 1. Parallel-mode EPR of **1** in toluene : dmf : EtOH (2 : 1 : drop) solution. Conditions: frequency, 9.37 GHz; $T = 9$ K; 20 mW microwave power.

Table 2. Selected bond lengths (Å) and angles (°) for H_2L^3.

N1–C11	1.291(3)
O1–C17	1.294(3)
O3–C16	1.372(3)
N2–C4	1.260(3)
O2–C10	1.338(3)
O4–C9	1.361(4)
N1–C1	1.457(3)
O3–C20	1.400(3)
N2–C3	1.468(3)
O4–C18	1.408(4)
C11–N1–C1	122.9(2)
N1–C1–C2	111.5(2)
N1–C11–C12	123.6(2)
C4–N2–C3	118.7(3)
N2–C3–C2	109.6(2)
N2–C4–C5	122.5(3)
O1–C17–C16	120.1(2)
O1–C17–C12	121.5(2)
O2–C10–C5	122.2(2)
O2–C10–C9	118.1(3)

of **1** recorded at 9 K (conditions: frequency, 9.37 GHz; 20 mW microwave power). Only the low-field portion of the spectrum is shown, since additional lines were not detected at higher fields. A well-resolved sextet signal centred at $g_{eff} = 8.1$ is observed, with a hyperfine splitting of $A_{||} = 44$ G.

The centre position of the sextet and hyperfine splitting for **1** are close to those previously reported for related μ-aquo-bridged Mn(III)–Schiff base complexes [6, 9, 28]. The small ^{55}Mn hyperfine coupling of 44 G is indicative of the electronic ground state $^5B_{1g}$, and thus this compound is either a five-coordinate distorted square-pyramidal complex or a six-coordinate distorted tetragonally elongated complex, with two axial O atoms from coordinated water molecules and two O and two N atoms from a tetradentate Schiff base ligand that is equatorially coordinated to the ion.

3.4. *Crystallographic studies*

3.4.1. Crystal structure of H_2L^3. Calculation of main bond lengths and angles of H_2L^3 are given in table 2. The structure of H_2L^3 consists of discrete molecules where two identical parts are twisted about the central aliphatic chain which acts as a spacer (figure 2). The N1–C11 and N1–C4 distances of 1.291(3) and 1.260(3) Å, respectively, are practically identical and consistent with C=N double bonding, indicating both imine groups fully localized in the molecule. The distance C17–O1 of 1.294(3) Å is considerably shorter than the C10–O2 distance of 1.34 Å; the last one fits the corresponding C–O distances for a single bond and, consequently, the former shows certain double-bond character. This behavior can be explained by the attraction of the phenol hydrogen (H1) by the neighboring nitrogen N1. This process is favored by the so-called "proton-sponge" effect [29, 30] which consists of the increase in the basicity of

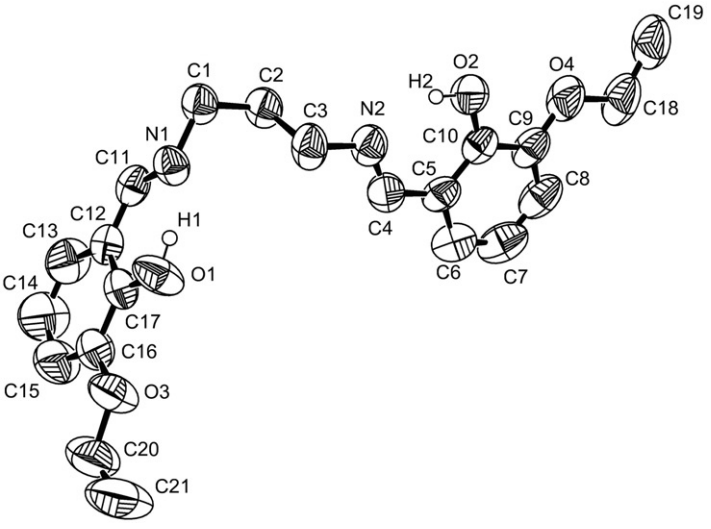

Figure 2. Molecular structure of H_2L^3 showing the atomic numbering scheme.

the imine nitrogens due to the spatial nearness of their lone pairs. The instability of a situation of proximity of these two lone pairs is then solved by the attraction of the proton from the hydroxy group by one of the nitrogen atoms. Despite the symmetry of the compound, the other imine/phenol pair does not show this phenomenon, just yielding a typical hydrogen bond interaction [H2 · · · N2 1.85(3) Å, O2 · · · N1 2.574(3) Å, and O2–H2 · · · N 147°]. Intermolecular interactions by hydrogen bonds can also be observed between the phenol oxygens of neighboring molecules.

The conformation of the free ligand in the solid state is of particular interest in relation to that required in a metal complex. Clearly, this conformation is not suitable for direct coordination to a metal ion in the usual arrangement for a tetradentate ligand. Therefore, significant rearrangement of the molecule must occur, involving rotation about the C2–C3 bond to give a near eclipsed conformation, for a mononuclear complexation.

3.4.2. Crystal structures of 1, 3, and 4. The structures of **1**, **3**, and **4** have been crystallographically solved. Main crystallographic data for these complexes are summarized in table 1, and bond lengths and angles are listed in table 3.

In all cases the geometry around the manganese ion can be described as distorted octahedral. An ORTEP view of **3** with the atomic numbering scheme is shown in figure 3. The coordination sphere around each manganese centre comprises the planar Schiff base ligand, tightly bound to the metal ion through the inner N_2O_2 compartment by the N_{imine} and O_{phenol} atoms (Mn–N_{imine} bond lengths of 1.97–2.05 Å and Mn–O_{phenol} of 1.87–1.89 Å which are typical of such complexes and corroborate the bisdeprotonation of the ligands [8, 31]), occupying the equatorial positions and giving rise to two six-membered chelate rings (which are nearly planar) and an additional five-, six-, or seven-membered chelate ring (depending on the diamine R). The axial positions of the octahedron are occupied by capping water molecules in all cases. The Jahn-Teller

Table 3. Selected bond lengths (Å) and angles (°) for **1**, **3**, and **4**.[a]

	1	**3A**	**3B**	**4**
Mn–O_p	1.8693(18)	1.885(5)	1.887(4)	1.8852(13)
	1.8705(17)	1.890(4)	1.894(5)	1.8910(13)
Mn–N_i	1.977(2)	2.038(4)	2.034(4)	1.9947(16)
	1.988(3)	2.050(4)	2.048(4)	1.9927(16)
Mn–O_{ax}	2.230(2)	2.205(4)	2.225(4)	2.2586(16)
	2.271(2)	2.243(4)	2.203(4)	2.2538(16)
O_p–Mn–O_p	92.92(8)	86.94(11)	87.06(11)	90.59(6)
O_p–Mn–N_i	92.92(9)	89.48(12)	89.00(14)	90.48(6)
	91.52(9)	89.26(12)	90.17(12)	90.48
	174.14(9)	174.96(11)	176.02(12)	176.92(6)
	175.28(9)	175.94(11)	176.78(11)	177.33(6)
N–Mn–N	82.64(11)	95.20(12)	87.6(2)	88.31(7)
O_a–Mn–O_a	176.11(8)	172.39(9)	174.50(10)	177.12(6)
Mn···Mn	4.912	5.073	5.073	5.160

[a]$O_p = O_{phenolic}$; $N_i = N_{iminic}$; $O_a = O_{axial}$.

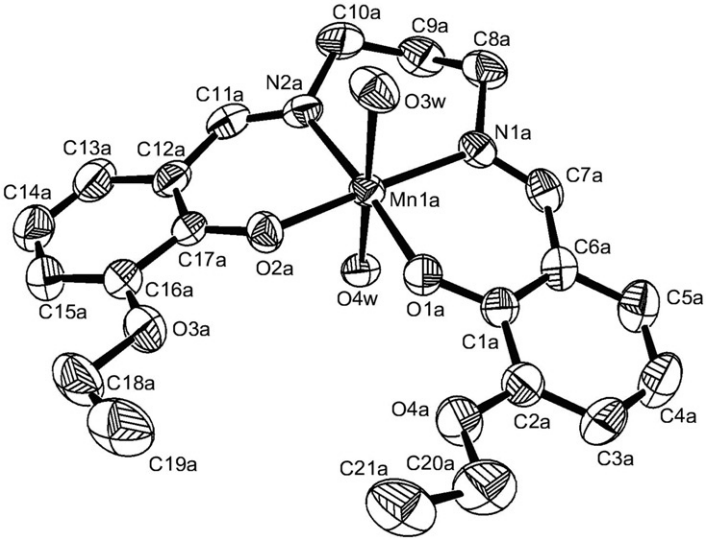

Figure 3. An ORTEP view of the environment around the manganese centre for **3**, including the atomic numbering scheme. Thermal ellipsoids are drawn at the 50% probability level. Hydrogens are omitted for clarity.

elongation expected for d^4 high-spin manganese(III) appears outstanding in the axis orthogonal to the plane of the Schiff base ligand, with distances ranging from 2.20 to 2.27 Å, considerably longer than the equatorial Mn–O bond lengths quoted earlier.

The deviation from an ideal octahedral geometry is also revealed by the range of angles observed around the metal centre (from 82.64° to 95.20°), as well as by the interaxial angle OW–Mn–OW of 172.39° to 177.12°.

In the case of **3** and **4**, disposition of the Schiff base ligand is not planar, and the two phenyl rings are located on the same (**3**) or different (**4**) (out)side of the N_2O_2

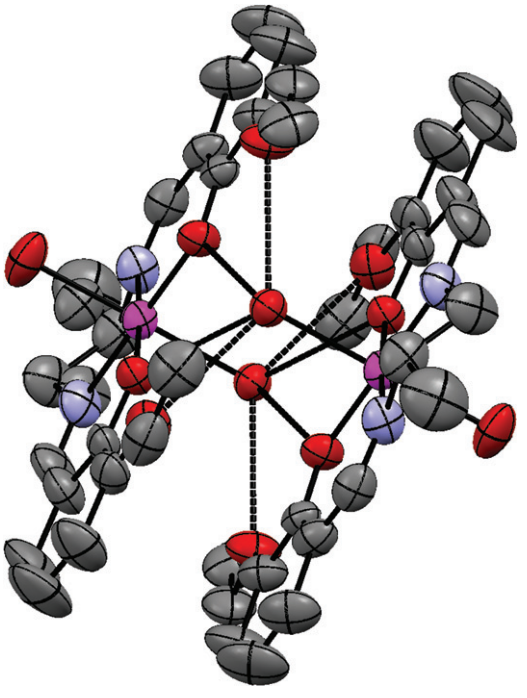

Figure 4. Molecular structure of **1**.

coordination site plane. The deviation from the Mn–N_2O_2 mean plane in such a way gives rise to a boat-shaped conformation for **3** or to a chair conformation in **4**, already observed in literature for similar cases [14, 32].

Moreover, the superstructure of the complexes involves associations via a combination of π-aryl offset interactions (3.71 to 3.89 Å) and hydrogen bonds between capping water molecules and both phenoxy and methoxy/ethoxy oxygens of neighboring Schiff base ligands, forming dimers in **1** and **3** and polymers in **4**. These hydrogen bonds are charge-assisted, that is, the hydrogen bond donor and/or acceptor carry positive and negative ionic charges, respectively, and hence are rather strong and short [33]. Complex **3** presents in the dimer two different molecules with Mn(1a)–Mn(1a), Mn(1b)–Mn(1b), with Mn–O_{phenol} and Mn–N_{imine} slightly different distances.

As a result of these supramolecular interactions, the Mn $\cdots$ Mn distances of about 4.70 Å for **1** and **3** are short for monomeric compounds; these types of $[MnL(H_2O)_2]_2^{2+}$ systems (being L Schiff base) have been previously reported by us [7–9, 28] as μ-aquo dimers (figure 4). These cationic $[MnL(H_2O)_2]_2^{2+}$ entities are electrostatically stabilized by nitrate counterions, which are hydrogen-bonding acceptors, interconneting the μ-aquo dimers and enriching the final supramolecular structure. The external apical water/methanol molecules of the dimers form two hydrogen bonds with two oxygens of nitrate; one of them is also bound to a methanol. Thus, there are two nitrate groups and two methanol molecules between μ-aquo dimers, generating a 1-D chain (figure 5).

The polymeric structure of **4** grows in one dimension, through hydrogen bonding between capping water molecules and both phenoxy and methoxy/ethoxy oxygens of the neighboring Schiff base ligands. In this case, nitrates and solvent water molecule

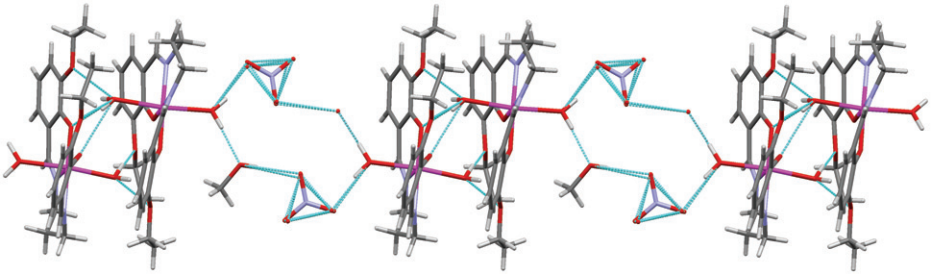

Figure 5. Stick diagram for **3** showing the hydrogen bonding between adjacent $[MnL^3(H_2O)_2]_2^{2+}$ dimeric units through nitrate anions and methanol solvent molecules.

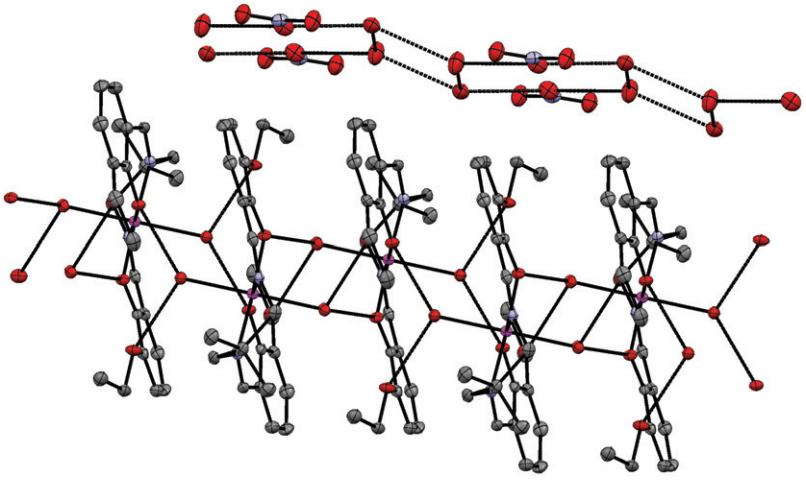

Figure 6. View along the *c*-axis of **4** showing the 1-D chains placing nitrates and solvent water molecules in channels. The chair conformation of the Schiff base ligand around the metal ion is also observed.

molecules connect through hydrogen bonds but they do not establish any of these interactions to the Mn–Schiff base moiety. This results in a 1-D Mn–Schiff base chain, parallel to a channel made up of the nitrate counterions and the water molecules (figure 6).

3.5. *Peroxidase and catalase studies*

The peroxidase-like activity of the complexes was followed by oxidation of the diammonium salt of 2,2′-azinobis(3-ethylbenzothiazoline)-6-sulfonic acid (ABTS) at pH 6.8 in aqueous solution. ABTS is colorless and reacts readily with H_2O_2 in the presence of a peroxidase catalyst to yield a stable, green radical cation $ABTS^{\bullet+}$ [34], which presents characteristic absorption bands at 415, 650, 735, and 815 nm. The extent of the reaction can be measured quantitatively at $\lambda = 650$ nm since $\varepsilon = 12{,}000\ (\text{mmol})^{-1}\,\text{cm}^{-1}$ has been determined. The oxidation potential of ABTS to provide $ABTS^{\bullet+}$ is invariable over a wide range of pH. In the absence of the complex, a solution of ABTS and H_2O_2 is

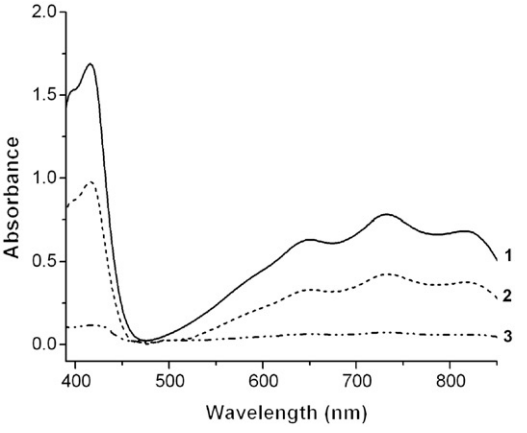

Figure 7. UV absorption spectra of **1**, **2**, and **3** recorded 10 min after injecting 10 μL of a 10^{-3} methanolic solution of the appropriate complex to 3 mL aqueous solution in the peroxidases probes. Blank spectra of ABTS + H_2O_2 and ABTS + complex, measured separately, show absorptions lower than **3**.

Table 4. Peroxidase and catalase activities for **1**–**5**.

	Catalysis	
Complex	Peroxidase[a]	Catalase[b]
1	33 ± 1	11 ± 1
2	24 ± 1	16 ± 1
3	2 ± 0.4	2 ± 0.4
4	2 ± 0.3	2 ± 0.4
5	2 ± 0.4	3 ± 0.4

[a]Peroxidase activity expressed as percentage of conversion of ABTS 10 min after mixing the solutions.
[b]Catalase activity expressed as percentage of H_2O_2 decomposed after 60 min.

stable for several hours without showing any formation of $ABTS^{\bullet+}$. The reaction of ABTS with H_2O_2 in the presence of **1** and **2** generates $ABTS^{\bullet+}$ and the characteristic absorption bands of this species could be established (figure 7; table 4). Further oxidation to the corresponding dication was not observed. Complexes **3**–**5** do not show significant peroxidase-like activity since the UV absorbances corresponding to the $ABTS^{\bullet+}$ radical cation are negligible in the assays with these complexes. The rate of formation of $ABTS^{\bullet+}$ of about 24–33% indicates a relevant peroxidase activity by **1** and **2** [7, 8].

We have also measured the stoichiometry of the disproportionation of H_2O_2 catalyzed by **1**–**5** by volumetric determination of the evolved O_2. Experiments were made in methanol. The experimental setup was evaluated by the measurements for the catalytic decomposition of H_2O_2 (2.5×10^{-3} mol) with MnO_2: *ca* 30 mL of dioxygen evolution was measured by a burette, which agrees with the calculated value based on the assumption that catalytic decomposition of H_2O_2 to H_2O and O_2 takes place. Table 4 collects the results of the catalase activities. Complexes **1** and **2** achieve

percentages of H_2O_2 dismutation from 11% to 16%, while **3**–**5** show considerably smaller percentages, with values lower than 3%.

Peroxidase and catalase studies clearly indentify two trends of catalytic behavior. Complexes **1** and **2** with a 2-membered alkyl chain spacer between the imine groups are active catalysts, while **3**–**5**, with 3- or 4-membered alkyl chains between the imine groups, do not present significant catalytic activities.

The dimeric nature of the complexes is decisive on their peroxidase activity since the oxidation of hydroperoxide to generate dioxygen involves an intramolecular two-electron transfer reaction, which is forbidden for a monomeric Mn(III) complex. The X-ray crystallographic studies reveal dimeric μ-aquo entities for **1**, which are able to perform a two one-electron redox process $[Mn^{III}, Mn^{III}] \rightarrow [Mn^{II}, Mn^{II}]$, while the polymeric structure of **4** probably gives monomeric complexes in solution, and therefore this type of complex may not mimic peroxidases. Self-assembly of the manganese complexes through hydrogen bonding arises as a key issue to enhance the peroxidase activity for this type of complex [28, 35].

However, **3** also has a dimeric structure but poor catalytic activity. This can be explained by the ability of these compounds to coordinate the substrate molecule. We have already proposed better catalytic behavior when the complex is able to easily coordinate the substrate molecule [7], and this is favored if the catalyst either has a vacancy in the coordination sphere or a labile ligand. The short two-carbon chain between imine groups in **1** and **2** constricts the chelate ring once nitrogens coordinate to the metal and leads to a tetragonally elongated octahedral geometry. An axial water molecule in this class of distorted geometries constitutes a quite labile ligand, which would generate a vacant position in the coordination sphere to accommodate the substrate molecule. On the other hand, the flexible three- or four-membered alkyl chain between the imine groups in the Mn compounds (**3**–**5**) favors a better stabilization of a high-symmetry octahedral geometry, which subsequently makes generation of a coordination site difficult.

4. Conclusions

This work further emphasizes the suitability of Schiff bases with inner and outer O–X ($X = CH_2CH_3$ in this work) groups for establishing rich hydrogen-bonding networks and shows that the counterion is a key factor in order to achieve supramolecular architectures.

The correlation of peroxidase and catalase activities of the complexes with the length of the spacer of the Schiff base should also be taken into account for designing new potential catalytic systems.

Supplementary material

CCDC 785921 (for H_2L^3), CCDC 786037 (for **1**), CCDC 786040 (for **3**), and CCDC 786042 (for **4**) contain the supplementary crystallographic data for this article.

These data can be obtained free of charge from The Cambridge Crystallographic Data Centre via http://www.ccdc.cam.ac.uk/

Acknowledgments

We thank Xunta de Galicia (09DPI004291PR) for financial support.

References

[1] C. Baleizao, H. Garcia. *Chem. Rev.*, **106**, 3987 (2006).
[2] F. Rosati, G. Roelfes. *ChemCatChem.*, **2**, 916 (2010).
[3] R. Li, F.P. Huang, X.J. Jiang, M.Y. Liu, Y.Y. Song, H. Liu, J.Y. Zhang. *J. Coord. Chem.*, **63**, 1611 (2010).
[4] J. Steinreiber, T.R. Ward. *Coord. Chem. Rev.*, **252**, 751 (2008).
[5] V. Calabrese, C. Cornelius, C. Mancuso, G. Pennisi, S. Calafato, F. Bellia. *Neurochem. Res.*, **33**, 2444 (2008).
[6] M. Maneiro, M.R. Bermejo, M.I. Fernandez, E. Gomez-Forneas, A.M. Gonzalez-Noya, A.M. Tyryshkin. *New J. Chem.*, **27**, 727 (2003).
[7] M.R. Bermejo, M.I. Fernandez, A.M. Gonzalez-Noya, M. Maneiro, R. Pedrido, M.J. Rodriguez, J.C. Garcia-Monteagudo, B. Donnadieu. *J. Inorg. Biochem.*, **100**, 1470 (2006).
[8] M.R. Bermejo, M.I. Fernandez, E. Gomez-Forneas, A. Gonzalez-Noya, M. Maneiro, R. Pedrido, M.J. Rodriguez. *Eur. J. Inorg. Chem.*, 3789 (2007).
[9] G. González-Riopedre, M.I. Fernández-García, A.M. González-Noya, M.A. Vázquez-Fernández, M.R. Bermejo, M. Maneiro. *Phys. Chem. Chem. Phys.*, **13**, 18069 (2011).
[10] H. Shyu, H. Wei, Y. Wang. *Inorg. Chim. Acta*, **290**, 8 (1999).
[11] G. Aromi, S. Bhaduri, P. Artus, K. Folting, G. Christou. *Inorg. Chem.*, **41**, 805 (2002).
[12] G. Morgan, K. Murnaghan, H. Muller-Bunz, V. Mckee, C. Harding. *Angew. Chem. Int. Ed.*, **45**, 7192 (2006).
[13] G. Fernandez, M. Corbella, G. Aullon, M. Maestro, J. Mahia. *Eur. J. Inorg. Chem.*, 1285 (2007).
[14] J.P. Costes, F. Dahan, B. Donnadieu, M.I. Fernandez-Garcia, M.J. Rodriguez-Douton. *Dalton Trans.*, 3776 (2003).
[15] V. Amendola, M. Boiocchi, B. Colasson, L. Fabbrizzi, M. Rodriguez-Douton, F. Ugozzoli. *Angew. Chem. Int. Ed.*, **45**, 6920 (2006).
[16] P.A. Gale, S.E. Garcia-Garrido, J. Garric. *Chem. Soc. Rev.*, **37**, 151 (2008).
[17] B. Notash, N. Safari, H.R. Khavasi. *Inorg. Chem.*, **49**, 11415 (2010).
[18] M. Maneiro, M.R. Bermejo, A. Sousa, M. Fondo, A.M. Gonzalez, A. Sousa-Pedrares, C.A. McAuliffe. *Polyhedron*, **19**, 47 (2000).
[19] G.M. Sheldrick. *SHELX-97 (SHELXS 97 and SHELXL 97), Programs for Crystal Structure Analyses*, University of Göttingen, Göttingen, Germany (1997).
[20] G.M. Sheldrick. *SADABS, Program for Scaling and Correction of Area Detector Data,* University of Göttingen, Göttingen, Germany (1996).
[21] W.J. Geary. *Coord. Chem. Rev.*, **7**, 81 (1971).
[22] D. Kong, Y. Xie. *Inorg. Chim. Acta*, **338**, 142 (2002).
[23] P. Przychodzen, M. Rams, C. Guyard-Duhayon, B. Sieklucka. *Inorg. Chem. Commun.*, **8**, 350 (2005).
[24] V. Daier, D. Moreno, C. Duhayon, J. Tuchagues, S. Signorella. *Eur. J. Inorg. Chem.*, 965 (2010).
[25] D. Pursche, M.V. Triller, C. Slinn, N. Redding, A. Rompel, B. Krebs. *Inorg. Chim. Acta*, **357**, 1695 (2004).
[26] J.A. Bonadies, M.L. Maroney, V.L. Pecoraro. *Inorg. Chem.*, **28**, 2044 (1989).
[27] E. Talsi, K. Bryliakov. *Mendeleev Commun.*, **14**, 111 (2004).
[28] A. Vázquez-Fernández, M.R. Bermejo, M.I. Fernández-García, G. González-Riopedre, M.J. Rodríguez-Doutón, M. Maneiro. *J. Inorg. Biochem.*, 2011, DOI: 10.1016/j.jinorgbio.2011.09.002.
[29] A.L. Llamas-Saiz, C. Foces, J. Elguero. *J. Mol. Struct.*, **328**, 297 (1994).
[30] D. Mekhatria, S. Rigolet, C. Janiak, A. Simon-Masseron, M.A. Hasnaoui, A. Bengueddach. *Cryst. Growth Des.*, **11**, 396 (2011).
[31] Q. Wu, Q. Shi, Y.G. Li, E.B. Wang. *J. Coord. Chem.*, **61**, 3080 (2008).

[32] M.R. Bermejo, M. Fondo, A. Garcia-Deibe, A.M. Gonzalez, A. Sousa, J. Sanmartin, C.A. McAuliffe, R.G. Pritchard, M. Watkinson, V. Lukov. *Inorg. Chim. Acta*, **293**, 210 (1999).
[33] H.A. Habib, B. Gil-Hernández, K. Abu-Shandi, J. Sanchiz, C. Janiak. *Polyhedron*, **29**, 2537 (2010).
[34] M. Zipplies, W. Lee, T. Bruice. *J. Am. Chem. Soc.*, **108**, 4433 (1986).
[35] W. Huang, J.X. Jiang, Z.Q. Feng, X.X. Kai, C.J. Hu, H. Yu, W. Yang. *J. Coord. Chem.*, **64**, 2101 (2011).